Energy Engineering

Tech Science Press

https://doi.org/10.32604/ee.2026.075769

ARTICLE

Hybrid Optimal Load Transfer for New Distribution Networks Coordinating Island Operation and Network Reconfiguration

Zhan Lv*, **Lan Lan**, **Zijian Hu**, **Honghua Xu**, **Hong Zhu** and **Jiehua Hou**

Nanjing Power Supply Company, State Grid Jiangsu Electric Power Co., Ltd., Nanjing, China

*Corresponding Author: Zhan Lv. Email: lvzhan15051818299@163.com

Received: 07 November 2025; Accepted: 13 January 2026; Published: 24 September 2026

ABSTRACT: To fully utilize the diverse source-grid-load-storage flexible resources integrated in new distribution networks, this paper proposes an optimal load transfer strategy that coordinates distributed generator island operation with network reconfiguration. Following a fault event, the strategy prioritizes the black-start capability of distributed generators and establishes island operation model to maximize and locally restore critical loads while respecting island operational constraints. To solve this model, the actual topology of the new distribution network is abstracted as a tree structure, and an improved Kruskal algorithm is employed to derive the minimum spanning tree, achieving optimal island partition for black-start distributed generators. Subsequently, for the residual network not included in the islands, a network reconfiguration model is formulated by considering multiple objectives including load loss minimization, network loss reduction, and switching operation optimization. Notably, to address the common limitations of existing methods in solving such complex, large-scale, and nonlinear optimization problems, the caterpillar fungus optimizer algorithm is adopted to efficiently and rapidly solve the proposed model. Finally, the effectiveness and superiority of the proposed load transfer strategy are validated using modified IEEE 33-bus and IEEE 123-bus test systems as representative new distribution networks. The comparative results demonstrate not only the performance advantages of the proposed strategy but also its practical applicability to distribution systems of different scales and complexities, offering a significant contribution to the field of reliability of power supply in the distribution network.

KEYWORDS: New distribution networks; load transfer strategy; island partition; network reconfiguration; caterpillar fungus optimizer

1 Introduction

To achieve the global carbon emission goal, the construction of new distribution networks is accelerating worldwide [1]. With the high-penetration integration of renewable power generation and various types of flexible resources [2], distribution networks have become increasingly complex and expansive in structure, posing significant challenges to their safe and economic operation [3]. Load transfer refers to the process of reliably and preferentially restoring power to critical loads after a distribution network fault by operating switches and optimizing the network topology, while also striving to meet the power demands of other affected loads as much as possible [4]. New distribution networks are expected to be low-carbon, clean, safe, reliable, efficient, and economical [5], with load transfer technology being a core enabler for achieving these goals. Therefore, it is necessary to research how to leverage the characteristics of various flexible source-grid-load-storage resources to participate in load transfer, thereby enhancing the power supply reliability of the distribution network [6].

In terms of the current research on optimal load transfer for distribution networks, tie lines are utilized in [7] to balance power loads across different areas of the distribution network, transferring loads from deficient feeder zones to zones with surplus supply capacity, achieving mutual power support between adjacent sections. The potential of high-voltage distribution networks is explored in [8], where network reconfiguration and load transfer are implemented in sectionalized distribution networks to improve overall power supply reliability. In [9], novel principles are proposed for switch operations during load transfer. The principles analyze the impact of switch operation sequences on transfer strategies to effectively control transfer risks. In [10], the regulatory role of energy storage, along with the network reconfiguration, is both considered to develop a coordinated load transfer method. Smart soft switches are studied in [11] to replace traditional tie switches, enabling flexible control of line power and ensuring safe load transfer. The control effect of step-voltage regulators (SVRs) is taken into account in [12], and the probabilistic distribution of voltage is utilized to optimize the output voltage of SVRs for achieving load transfer in distribution networks.

The aforementioned studies demonstrate considerable practical value in load transfer. However, they primarily focus on distribution network topology reconfiguration and fail to fully exploit the potential of flexible resources. The IEEE 1547-2004 standard expands the specifications for interconnecting distributed generators (DGs) with power systems, leveraging the island operation capability of DGs that can serve as black-start sources to ensure power supply to outage loads [13]. Various DGs in new distribution networks, such as micro turbines (MTs), energy storage batteries (ESBs), and diesel engines (DEs), possess black-start capabilities, contributing to stable power supply after distribution network faults [14]. Meanwhile, flexible loads are widely present as adjustable resources in new distribution networks, which can be regulated during fault conditions [15].

To construct and solve the models of optimal load transfer, common methods include mathematical programming, heuristic algorithm, and artificial intelligence. For mathematical programming, load transfer models based on mixed-integer second-order cone programming and mixed-integer linear programming are proposed in [16,17], respectively. These methods indicate high performances, but directly solvable models are difficult to construct due to the increasing complexity of distribution networks. For heuristic algorithms, heuristic rules are developed in [18] to operate corresponding tie switches for load transfer. In [19], binary particle swarm optimization algorithm is proposed to solve the load transfer model, but is prone to local optima. For artificial intelligence methods, an optimal load transfer strategy is developed in [20] based on deep reinforcement learning. In [21], hybrid reinforcement learning is employed to enhance the optimization performance of intelligent agents but sacrifices some optimality. In summary, among existing methods, traditional solving techniques struggle to adapt to large-scale, nonlinear, and complex distribution network models. Commonly used heuristic methods require further improvement in solving efficiency, while artificial intelligence methods often sacrifice a certain level of solution accuracy. Consequently, there is a need to balance optimization effectiveness with solving efficiency. It is essential to meet the real-time requirements of modern power systems while ensuring optimization performance, thereby adapting to large-scale load transfer in new distribution networks, reducing outage durations, and safeguarding customer power supply.

In summary, to address the research gaps in exploiting potential of novel distribution networks, this study considers various new resources and establishes a load transfer model coordinating island operation and network reconfiguration. The framework of the proposed load transfer strategy is shown in Fig. 1. During a distribution network fault, an improved Kruskal algorithm is first used to partition islands for DGs with Island operation capabilities, in order to prioritize the restoration of power supply for critical loads. Afterwards, a network reconfiguration model is established for the remaining network, while a novel caterpillar fungus optimizer (CFO) algorithm is employed to solve the proposed model, achieving power supply for the remaining loads. Finally, a modified IEEE 33-bus system and IEEE 123-bus test systems are adopted as representative new distribution network cases to simulate fault scenarios, validating the effectiveness and real-time performance of the proposed load transfer model for power supply restoration.

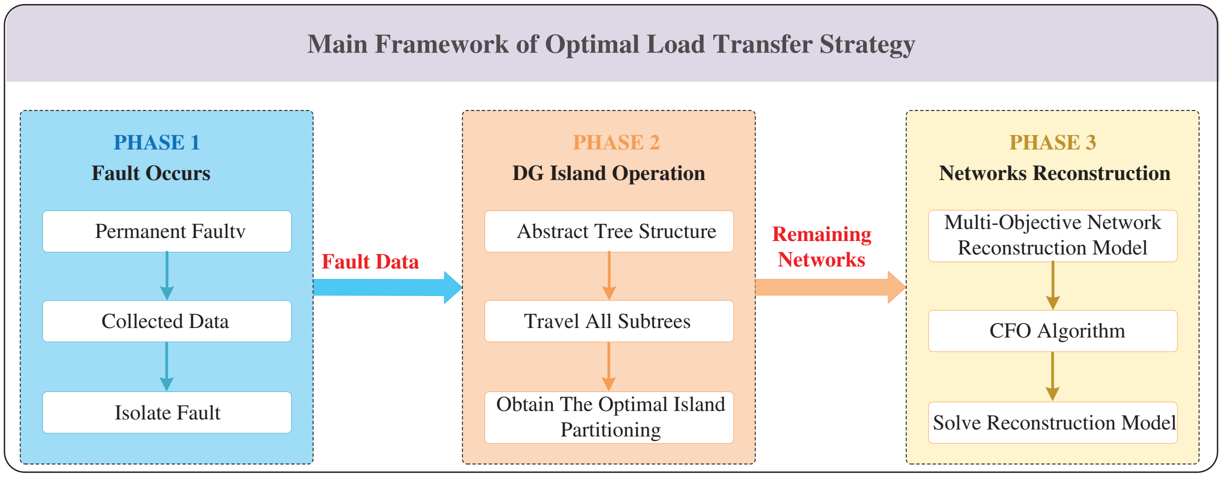

Figure 1: Main framework of proposed load transfer strategy.

The major contributions of this study are summarized as follows:

(1) A novel hybrid load transfer framework is proposed for distribution networks to maximize reliable power supply to loads by coordinating stages of distributed power generation island operation and network reconfiguration. The black-start capability of distributed generation is considered to prioritize the restoration of important load power supply. By combining the two stages, power supply reliability can be greatly improved.
(2) An optimal island partitioning method of distribution networks is developed based on improved Kruskal algorithm for black-start distributed power sources. The actual topology is abstracted as a tree structure in the method to solve the minimum spanning tree problem, achieving optimal island partitioning of those black-start distributed sources and effectively restoring important loads.
(3) A novel multi-objective network reconfiguration model is established considering system operating with islands of distributed sources, along with an efficient solution method namely CFO algorithm. For the remaining networks that are not included in the island, the network model comprehensively considers the minimum load loss, network loss reduction, and switching operation.

2 Island Operation Strategy for New Distribution Networks Considering Flexible Resources

2.1 Mathematical Model of DGs Output Characteristics

2.1.1 Mathematical Model of Distributed Photovoltaic Output Characteristics

The output power of photovoltaic (PV) systems depends on their module area and real-time irradiance, as presented in equations below [22]:

$$P_{\mathrm{pv},t} = \begin{cases} AP_{\mathrm{std}}\dfrac{S_t^2}{S_{\mathrm{std}}k_c}, & 0 \le S_t < S_c \\ AP_{\mathrm{std}}\dfrac{S_t}{S_{\mathrm{std}}}, & S_c \le S_t < S_{\mathrm{std}} \\ AP_{\mathrm{std}}, & S_t \ge S_{\mathrm{std}} \end{cases}, \tag{1}$$

where $P_{\mathrm{pv},t}$ represents the PV output power at time t, A denotes the PV module area, P_{std} signifies the rated PV output power, S_t and S_{std} correspond to the instantaneous irradiance and rated irradiance at time t, and S_c is a specific irradiance threshold. When the real-time irradiance S_t is less than S_c, the PV output has a nonlinear relationship with irradiance; Conversely, once S_t reaches or exceeds S_c, the PV output changes linearly with irradiance.

2.1.2 Mathematical Model of Common Controllable Distributed Generators Output Characteristics

MTs and DEs must satisfy power constraints and ramp rate constraints, expressed as follows:

$$P_{\mathrm{DG},i}^{\min} \le P_{\mathrm{DG},i,t} \le P_{\mathrm{DG},i}^{\max}, \tag{2}$$

$$Q_{\mathrm{DG},i}^{\min} \le Q_{\mathrm{DG},i,t} \le Q_{\mathrm{DG},i}^{\max}, \tag{3}$$

$$-R_{\mathrm{DG},i}^{P_l} \le P_{\mathrm{DG},i,t} - P_{\mathrm{DG},i,t-1} \le R_{\mathrm{DG},i}^{P_u}, \tag{4}$$

$$-R_{\mathrm{DG},i}^{Q_l} \le Q_{\mathrm{DG},i,t} - Q_{\mathrm{DG},i,t-1} \le R_{\mathrm{DG},i}^{Q_u}, \tag{5}$$

where $P_{\mathrm{DG},i,t}$ and $Q_{\mathrm{DG},i,t}$ are the active and reactive power output of the DG connected to bus i at time t, respectively; $P_{\mathrm{DG},i}^{\max}$, $P_{\mathrm{DG},i}^{\min}$, $Q_{\mathrm{DG},i}^{\max}$, $Q_{\mathrm{DG},i}^{\min}$ are the corresponding upper and lower limits of active and reactive power output; $R_{\mathrm{DG},i}^{P_u}$, $-R_{\mathrm{DG},i}^{P_l}$, $R_{\mathrm{DG},i}^{Q_u}$, $-R_{\mathrm{DG},i}^{Q_l}$ are the upper and lower limits of the ramp rates for active and reactive power control of the DG; $P_{\mathrm{DG},i,t-1}$, $P_{\mathrm{DG},i,t}$, $Q_{\mathrm{DG},i,t-1}$, $Q_{\mathrm{DG},i,t}$ are the active and reactive power outputs of the DG at adjacent time steps.

ESBs must satisfy charging/discharging constraints and energy constraints, as shown below:

$$v_{i,t}P_i^{\mathrm{bess,min}} \le P_{\mathrm{c},i,t}^{\mathrm{bess}} \le v_{i,t}P_i^{\mathrm{bess,max}}, \tag{6}$$

$$u_{i,t}P_i^{\mathrm{bess,min}} \le P_{\mathrm{d},i,t}^{\mathrm{bess}} \le u_{i,t}P_i^{\mathrm{bess,max}}, \tag{7}$$

$$u_{i,t} + v_{i,t} \le 1, \tag{8}$$

$$S_{i,t} = S_{i,t-1} + \frac{\eta_i^{\mathrm{c}} P_{\mathrm{c},i,t}^{\mathrm{bess}} \Delta t - P_{\mathrm{d},i,t}^{\mathrm{bess}} \Delta t / \eta_i^{\mathrm{d}}}{E_{\mathrm{N}}}, \tag{9}$$

$$S_i^{\min} \le S_{i,t} \le S_i^{\max}, \tag{10}$$

where $P_{\mathrm{c},i,t}^{\mathrm{bess}}$ and $P_{\mathrm{d},i,t}^{\mathrm{bess}}$ are the charging and discharging power of the energy storage connected to bus i at time t, respectively; $P_i^{\mathrm{bess,max}}$ and $P_i^{\mathrm{bess,min}}$ are the upper limits of charging and discharging power; $v_{i,t}$ and $u_{i,t}$ are the charging and discharging status variables; η_i^{c} and η_i^{d} are the charging and discharging efficiencies, respectively; $S_{i,t-1}$ and $S_{i,t}$ are the energy levels of the storage at adjacent time steps; $S_i^{\max}$ and $S_i^{\min}$ are the lower and upper limits of the energy storage capacity.

2.2 Mathematical Model of Load Power Characteristic

This paper analyzes load characteristics from the perspectives of importance and controllability.

- Load importance: Due to their different characteristics, the consequences of power interruption vary among loads. Loads are generally classified into three levels based on the severity of interruption consequences: first-class load, second-class load, third-class load. Higher-level loads cause more adverse consequences in terms of personal safety and economic losses during outages. Therefore, they should be prioritized during load transfer to ensure power supply [23].
- Load controllability: Based on participation in demand response, loads can be categorized into non-controllable loads and flexible loads. Non-controllable loads are fixed loads in the power system and

cannot be regulated. Flexible loads can be actively adjusted according to power demand and can participate in load transfer as adjustable resources in emergencies. The constraints are as follows [24]:

$$(1 - K_{i,\mathrm{P}}) * P_{i,\mathrm{D0}} \leq P_{i,\mathrm{D}} \leq (1 + K_{i,\mathrm{P}}) * P_{i,\mathrm{D0}}, \tag{11}$$

$$(1 - K_{i,\mathrm{Q}}) * Q_{i,\mathrm{D0}} \leq Q_{i,\mathrm{D}} \leq (1 + K_{i,\mathrm{Q}}) * Q_{i,\mathrm{D0}}, \tag{12}$$

where $P_{i,\mathrm{D0}}$ and $Q_{i,\mathrm{D0}}$ are the initial active and reactive load power at bus i; $K_{i,\mathrm{P}}$ and $K_{i,\mathrm{Q}}$ are the proportions of flexible active and reactive load; $P_{i,\mathrm{D}}$ and $Q_{i,\mathrm{D}}$ are the active and reactive load power after flexible load control.

2.3 Island Partitioning for New Distribution Networks Based on Improved Kruskal Algorithm

2.3.1 Principles of Island Partitioning

This paper considers the following four principles for island partitioning:

- Priority for important loads. Based on load importance levels, different weights are assigned to first-class load, second-class load, third-class load to ensure that load with higher weight are restored first during load transfer.
- Full utilization of dg capacity. When partitioning islands, the load allocated to DG should match its capacity, ensuring the safe operation of the DGs while minimizing outage load.
- Minimum network losses. Given the limited capacity of DGs, network losses need to be reduced during island operation to provide sustained and maximum power supply.
- Limited switching operations. To extend switch lifespan and ensure operational safety, frequent switch operations should be avoided, and the number of switching actions should be minimized.

2.3.2 Mathematical Model of Island Partitioning

Using DGs as the power source for load buses within islands, the objective function comprehensively considers restoring power to important loads and the electrical distance between DGs and load buses:

$$\max f = \sum_{j=1}^{n} \sum_{i=1}^{m} \frac{\chi_i P_{i,t}}{D_{ji}}, \tag{13}$$

where n is the number of formed islands, m is the number of load buses, χ_i is the weight of the load, $P_{i,t}$ is the active load at bus i at time t, and D_{ji} is the electrical distance between the DG j and load bus i. A larger electrical distance will result in more power transmission losses.

The constraints that need to be satisfied include:

- Island power constraint

To ensure island security, the adjustable capacity of the DG should be greater than the total load within the island, constrained as follows:

$$\sum_{j=1}^{q} P_{j,t} \geqslant \sum_{i \in D} P_{i,t}, \tag{14}$$

where q is the number of DGs within the island, D is the set of load buses, $P_{j,t}$ is the output of the DG j at time t, and $P_{i,t}$ is the active load bus i at time t.

- Island power flow constraints

Active and reactive power flow constraints are as follows:

$$P_{i,t} - U_{i,t} \sum_{j=1}^{n} U_{j,t} \left(G_{ij} \cos \delta_{ij,t} + B_{ij} \sin \delta_{ij,t} \right) = 0, \tag{15}$$

$$Q_{i,t} - U_{i,t} \sum_{j=1}^{n} U_{j,t} \left(G_{ij} \cos \delta_{ij,t} + B_{ij} \sin \delta_{ij,t} \right) = 0, \tag{16}$$

where $P_{i,t}$ and $Q_{i,t}$ are the active and reactive power injection at bus i at time t, respectively; $U_{i,t}$ and $U_{j,t}$ are the voltage magnitudes of bus i and j at time t, respectively; $\delta_{ij,t}$ is the voltage phase angle difference between bus i and j at time t; G_{ij} and B_{ij} are the conductance and susceptance of line ij.

- Security operation constraints

Including line capacity constraints, power transmission constraints, and bus voltage constraints are as follows:

$$\left(P_{ij,t}^2 + Q_{ij,t}^2 \right) / U_{i,t}^2 \leq I_{ij,\max}^2, \tag{17}$$

$$P_{ij,t}^2 + Q_{ij,t}^2 \leq S_{ij,\max}^2, \tag{18}$$

$$U_i^{\min} \leq U_{i,t} \leq U_i^{\max}, \tag{19}$$

where $P_{ij,t}$ and $Q_{ij,t}$ are the active and reactive power flowing through line ij at time t, respectively; $I_{ij,\max}$ and $S_{ij,\max}$ are the current carrying capacity and transmission capacity upper limit of line ij; $U_i^{\max}$ and $U_i^{\min}$ are the lower and upper voltage limits at bus i.

For the line thermal capacity constraints, this paper further evaluates the load-carrying capacity of the lines:

Firstly, based on the thermal equilibrium equation of the line, the thermal capacity of line ij can be expressed as:

$$C_{ij,\max} = \sqrt{\frac{q_c + q_r - q_s}{R\left(T_c\right)}}, \tag{20}$$

where q_c represents convective heat dissipation, q_r denotes radiative heat dissipation, q_s is solar heat absorption, $C_{ij,\max}$ is the thermal capacity of line and $R\left(T_c\right)$ indicates the unit resistance per length of the conductor at temperature T_c.

Subsequently, the remaining capacity of line ij can be represented as:

$$\Delta S_{ij} = \sqrt{3} \cdot U_0 \cdot \left(C_{ij,\max} - I_{ij} \right), \tag{21}$$

where U_0 is the rated voltage of line ij, I_{ij} is the magnitude of current in line ij.

Finally, the safety margin of the line ij is:

$$\eta_{ij} = \frac{\Delta S_{ij}}{S_{ij,\text{rated}}} \times 100\%, \tag{22}$$

where $S_{ij,\text{rated}}$ is the rated capacity of line ij.

η_{ij} needs to be greater than or equal to the safety threshold λ, as follows:

$$\eta_{ij} \geq \lambda, \tag{23}$$

- Network topology constraint

The partitioned islands must remain radial without forming loops:

$$B_i \in G, \tag{24}$$

where B_i is the formed network topology i, and G is the set of radial networks.

2.3.3 Island Partitioning Algorithm Based on Improved Kruskal Algorithm

Distribution networks are designed with a closed-loop structure but operate in an open-loop mode, resulting in a radial topology. Therefore, the actual topology can be abstracted into a tree with the system power source as the root and loads as leaf buses. Additionally, buses with DGs are treated as leaf buses with power source characteristics, without altering the system structure. Fig. 2 shows the actual topology of a typical new distribution network, and its abstraction into a tree connection diagram is shown in Fig. 3. As can be seen, the tree in Fig. 3 is divided into 5 layers according to the power flow direction. The hierarchy and directionality of the tree simulate the sequence of bus load transfer, ensuring orderly transfer. The tree formed by the connection graph is defined as: $T = (V, E)$. T is the binary representation of the tree; V is the vertex set, containing n vertices $\{V_1, V_2, \cdots V_n\}$; E is the edge set, containing the weights of the edges connecting the n vertices, such as: V_{ij} represents the edge connecting vertices V_i and V_j, with a corresponding weight of W_{ij}.

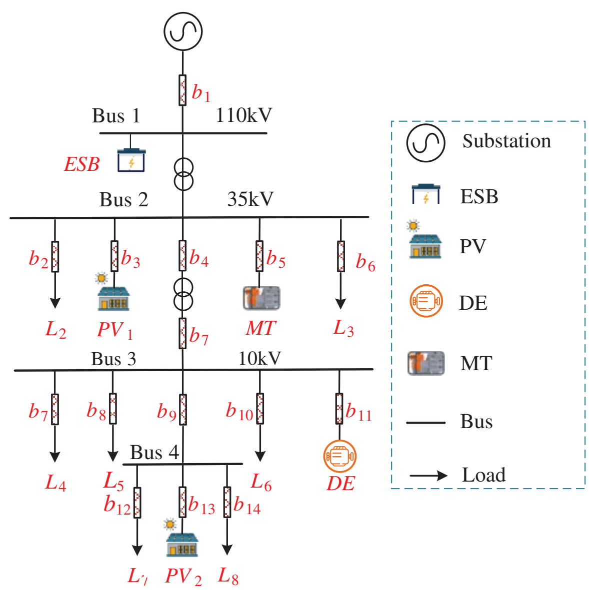

Figure 2: Typical topology of new distribution network.

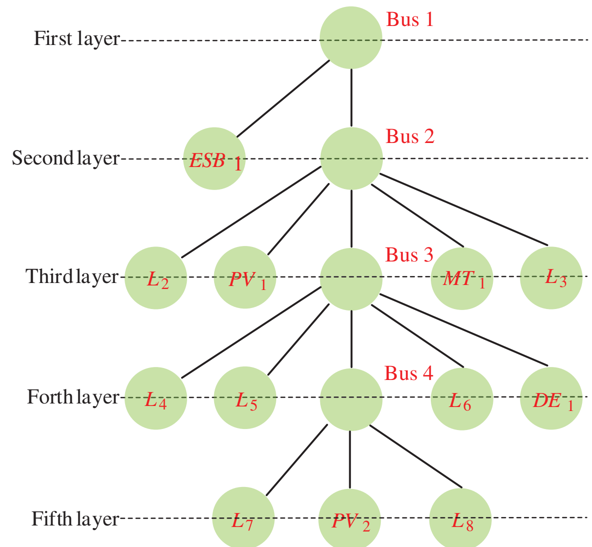

Figure 3: Connection diagram of new distribution network.

Traversing all edge combinations of tree T can yield all subtrees. To achieve the objective function in Eq. (1), which aims to maximize the restoration of important loads, the minimum spanning tree algorithm is used for Island partitioning. This algorithm uses edge weight W_{ij} to find the minimum spanning tree. First, it is necessary to assign weights to the edges of the connection graph. For two load bus i and j with load powers P_i and P_j, load weights χ_i and χ_j, the weight W_{ij} of edge V_{ij} can be assigned as:

$$W_{ij} = \frac{1}{\chi_i P_i + \chi_j P_j}, \tag{25}$$

where W_{ij} represents the importance of edge V_{ij}, determined by load bus i and j. When the load bus i and j are more important, this value is smaller, conforming to the operation rules of the minimum spanning tree, thereby ensuring that important loads in the spanning tree are restored first.

The Kruskal algorithm is a search algorithm that employs a greedy strategy to construct the minimum spanning tree of a connected graph. It is particularly suitable for finding the minimum spanning tree of relatively sparse connected graphs. The algorithmic principle is driven by starting from an initial state and making decisions based on the current local optimum, aiming to achieve the steepest ascent or descent of the objective function while satisfying constraint equations. Specifically, the algorithm iteratively selects the shortest edge from the candidate set and adds it to the vertex and edge sets of the selected subgraph until all nodes are traversed.

However, the traditional Kruskal algorithm cannot guarantee the uniqueness of the solution and various operational constraints of the distribution network must be considered during the search process. Therefore, corresponding modifications to the Kruskal's algorithm are imperative. This involves resetting the search starting point, modifying search conditions and order, adding constraint checks, etc., to perform island partitioning for the new distribution network [25]. The algorithm flow is as follows:

- Input the distribution network topology, system parameters, and load sizes, correct DGs with black-start capability, convert the actual topology into a tree connection graph, and calculate the weights of all edges.

- After connecting each DG to its adjacent bus, link those buses not directly connected to any DG bus to the nearest DG-connected bus based on minimum edge weight in ascending order of bus numbers. This forms initial islands, each consisting of several buses and one DG only.
- Define the evaluation function $G = \sum_{j=1}^{q} P_{j,t} - \sum_{i \in D} P_{i,t}$ according to Eq. (14). For each initial island, integrate loads sequentially by priority level (first-, second-, and third-level loads). Arrange the n-level ($n = 1, 2, 3$) load bus in ascending order of edge weight and incorporate them one by one. After adding each load, verify the evaluation function. If $G > 0$ is satisfied, update the vertex set and edge set and proceed to the next load until $G \leq 0$ is met. Repeat for all islands in numerical order.
- Define the evaluation function $H = \eta_{ij} = \frac{\Delta S_{ij}}{S_{ij,\text{rated}}} \times 100\%$ according to Eq. (20). For islands where $G \leq 0$, if there remain n-level loads not yet integrated, connect the island to another island with a function value greater than zero via the minimum-weight edge, then repeat step (3). If $G > 0$, directly update the vertex and edge sets and continue integrating loads until all n-level loads are included or $G \leq 0$. If $H \leq \lambda$, adjust the corresponding line, add a line and reduce the load power transmission until $H > \lambda$.
- Verify that the island partition scheme satisfies all constraints of the island model, including network power flow constraints Eqs. (15) and (16), security constraints Eqs. (17)–(23), network topology constraint Eq. (24), distributed generator constraints Eqs. (2)–(10), and flexible load constraints Eqs. (11) and (12).
- When the connection graph completes the above steps, if there are still buses not connected to any load, delete them. The optimized T is the island partitioning result for the first stage of load transfer.

For an explicit illustration, the pseudo-code of improved Kruskal algorithm for island partitioning is provided in Table 1.

Table 1: Pseudo-code of improved Kruskal algorithm.

Algorithm 1: Improved kruskal algorithm for island partitioning

```
Convert the actual topology of new distribution network into a weighted connected diagram;
Determine the number N, evaluation function G and H;
FOR i = 1: N
  IF G > 0
    FOR i = j: 3
      Execute the integration operation for j − level load;
      Verify operational constraints and ensure H > λ;
    END FOR
      Optimize the minimum spanning tree;
  END IF
END FOR
```

3 Network Reconfiguration for New Distribution Networks Based on CFO

3.1 Network Reconfiguration Model for New Distribution Networks

3.1.1 Objective

Following a fault in the distribution network, island partitioning is first performed to leverage the black-start capability of DGs and prioritize restoration of critical loads. For remaining buses, network reconfiguration methods are employed—connecting buses to the main grid via tie switches—enabling the main grid to supply residual loads and ensure continuous service. The objectives of network reconfiguration encompass: minimizing load curtailment, reducing network losses, and limiting switch operations, as detailed below:

$$\min F = \mu_1 f_1 + \mu_2 f_2 + \mu_3 f_3, \tag{26}$$

$$f_1 = \sum_{i=1}^{N} u_i \chi_i P_{i,t}, \tag{27}$$

$$f_2 = \sum_{i=1}^{m1} (1 - B_i) + \sum_{j=1}^{m2} C_j, \tag{28}$$

$$f_3 = \sum_{ij \in \mathcal{L}} \left(P_{ij,t}^2 + Q_{ij,t}^2 \right) R_{ij} / U_{i,t}^2, \tag{29}$$

where F is the total objective function; f_1, f_2, f_3 are the sub-objective functions for total lost load, number of switching operations, and network losses, respectively; μ_1, μ_2, μ_3 are the weight coefficients for the sub-objective functions f_1, f_2, f_3; N is the number of buses in the network undergoing reconfiguration; u_i is the indicator coefficient defined for each bus: $u_i = 0$ indicates that the load bus i is under normal power supply, while $u_i = 1$ signifies a state of load outage; χ_i is the load weight; $P_{i,t}$ is the active load of bus i at time t; m_1 and m_2 are the total numbers of branch switches and tie switches in the network, respectively; B_i and C_j represent the status (on/off) of branch switch and tie switch, respectively; $P_{ij,t}$, $Q_{ij,t}$ are the active power and reactive power of line ij at time t, respectively; R_{ij} is resistance of line ij; $U_{i,t}$ is the voltage magnitude at bus i at time t. This paper considers minimizing lost load as the primary objective and number of switching operations and network losses as secondary objectives, hence setting $\mu_1 = 0.6$, $\mu_2 = 0.3$, $\mu_3 = 0.1$ [26], which can be adjusted as needed. For branch switch and tie switch, branch switches are normally closed, while tie switches are normally open, setting 1 for a closed state and 0 for an open state.

3.1.2 Constraints

The constraints include network power flow constraints Eqs. (15) and (16), security constraints Eqs. (17)–(23), network topology constraint Eq. (24), distributed generator constraints Eqs. (2)–(10), and flexible load constraints Eqs. (11) and (12).

3.2 Solving the Network Reconfiguration Model Based on CFO

3.2.1 Principle of CFO

CFO is a novel intelligent optimization approach inspired by the parasitic mechanisms of caterpillar fungus, designed for rapid resolution of complex nonlinear optimization problems [27]. The natural host of caterpillar fungus is the Hepialus larvae. The host experiences infection when caterpillar fungus ascospores germinate to form branched bud tubes that penetrate the host's body and propagate mycelium. During host selection, caterpillar fungus emulates a stochastic search mechanism, dynamically adjusting exploration pathways in response to environmental variations. This dual-directional search exhibits multifactor-driven characteristics—modeled as the wave advance operator (horizontally) and spiral rising operator (vertically), mimicking the spatial host-seeking behavior of caterpillar fungus.

When modeling the exploration mechanism of caterpillar fungus, three modeling principles are introduced. First, each ascospore capsule produces only one ascospore, and each ascospore can infect only one host larva. Successful parasitism requires two attempted infections per caterpillar fungus individual, capturing behavioral stochasticity. The total number of infected larvae remains constant, imposing dynamic population constraints.

- Search operators

During the exploratory phase, caterpillar fungus individuals are ranked in descending order based on initial fitness values. They randomly select exploration directions, with equal probability allocated to horizontal and vertical orientations to ensure omnidirectional exploration.

Horizontally, the algorithm exhibits undulatory propulsion, simulating the natural horizontal diffusion behavior of caterpillar fungus. The search trajectory features nonlinear and periodic oscillatory characteristics, enabling wide-area optimization—this mechanism is termed the wave advance operator, defined as follows:

$$X_{\mathrm{CF},i}^{\mathrm{so}} = \begin{cases} X_{\mathrm{CF},i} - r_1 \times \{X_{\mathrm{best}} - X_{\mathrm{CF},i}\} + \alpha \times \{X_{\mathrm{best}} - X_{\mathrm{CF},i}\}, & i = 1 \\ X_{\mathrm{CF},i} - r_1 \times \{X_{\mathrm{CF},i-1} - X_{\mathrm{CF},i}\} + \alpha \times \{X_{\mathrm{best}} - X_{\mathrm{CF},i}\}, & i = 2, 3, \ldots, N \end{cases}, \tag{30}$$

where $X_{\mathrm{CF},i}^{\mathrm{so}}$ is the position of the ith caterpillar fungus during the exploration process in the horizontal direction; r_1 is a random number within $[0, 1]$; X_{best} is the position of the caterpillar fungus with the minimum fitness; $X_{\mathrm{CF},i}$ and $X_{\mathrm{CF},i-1}$ are the positions of the ith and $(i-1)$ th caterpillar fungus, respectively. Since the initial state of caterpillar fungus is sorted in descending order of fitness, the performance of the $(i-1)$ th caterpillar fungus is better than that of the ith one. The horizontal search step size α is calculated as follows:

$$\alpha = 2.5 * r_2 * |\cos(\pi * r_2)|, \tag{31}$$

where r_2 is a random number within $[0, 1]$; α represents the random search step length of the caterpillar fungus, enabling efficient search in the feasible space and improving optimization efficiency.

Vertically, the caterpillar fungus exhibits spiral ascent exploration, described by the spiral rising operator as follows:

$$X_{\mathrm{CF},i}^{\mathrm{so}} = \begin{cases} X_{\mathrm{best},i} - r_3 \times (X_{\mathrm{best}} - X_{\mathrm{CF},i}) + \beta \times (X_{\mathrm{best}} - X_{\mathrm{CF},i}), & i = 1 \\ X_{\mathrm{best}} - r_3 \times (X_{\mathrm{CF},i-1} - X_{\mathrm{CF},i}) + \beta \times (X_{\mathrm{best}} - X_{\mathrm{CF},i}), & i = 2, 3, \ldots, N \end{cases}, \tag{32}$$

where r_3 is a random number within $[0, 1]$; The vertical search step size β is calculated as follows:

$$\beta = 2 \times \cos(\pi \times r_4) \times \left| \left(\frac{iteration}{Max\_iteration} \right)^{r_4 \times r_5} \right|, \tag{33}$$

where r_4 denotes a random number uniformly distributed within [0,1]; r_5 is an integer randomly selected for each individual across the entire population, and $r_5 \in \{1, 2\}$; $iteration$, $Max\_iteration$ represent the current *iteration* count and maximum allowable iterations, respectively; The coefficient $(iteration/Max\_iteration)^{r_4 \times r_5}$ defines the search radius for local exploration around each caterpillar fungus individual. Furthermore, when $r_5 = 2$, smaller radius enable fine-grained searches within confined regions; as the $iteration$ number approaches the $Max\_iteration$, this coefficient tends towards 1, implementing an adaptive scaling strategy. This progressive adjustment expands the search scope when convergence toward local optima occurs, thereby enhancing the algorithm's capability to escape suboptimal solutions during late iteration phases.

- Larva parasitism

During parasitic stage, caterpillar fungus exhibits strategic selection between re-parasitism and optimal parasitism, facilitating convergence toward higher parasitic success rates.

Re-parasitism mechanism: While maintaining parasitic association with the same host larva, the latter may be re-infected by a caterpillar fungus individual possessing superior fitness values. This mechanism enhances parasitic reliability, described as follows:

$$X_{\mathrm{CF},i}^{\mathrm{pl}} = X_{\mathrm{CF},i}^{\mathrm{so}} + 3 \times r_6 \times \left(X_{\mathrm{best}} - X_{\mathrm{CF},i}^{\mathrm{so}}\right), i = 1, 2, \ldots, N, \tag{34}$$

where $X_{\mathrm{CF},i}^{\mathrm{pl}}$ represents the parasitic stage of the ith caterpillar fungus individual; r_6 denotes a random number drawn from the standard normal distribution, independently generated and assigned to each individual. Since r_6 predominantly clusters near zero, it induces minor perturbations in the caterpillar fungus positions most of time. However, when r_6 attains larger magnitudes, significant displacements occur, propelling individuals into unexplored regions and mitigating entrapment in local optimums.

Optimal parasitism: Unlike re-parasitism, optimal parasitism mainly occurs when a caterpillar fungus encounters an already parasitized larva. The caterpillar fungus tends to choose the best growth environment, described as:

$$X_{\mathrm{CF},i}^{\mathrm{pl}} = X_{\mathrm{best}} + 3 \times \lambda \times \left(X_{\mathrm{best}} - X_{\mathrm{CF},i}^{\mathrm{so}}\right), i = 1, 2, \ldots, N, \tag{35}$$

$$\lambda = r_7 \times \left(\frac{iteration}{Max\_iteration} - 1\right)^2, \tag{36}$$

where r_7 is a random number uniformly distributed within $[0, 1]$; λ signifies the search step size, which is initially large during early iterations and progressively decreases with increasing iteration counts, ultimately approaching zero. This adaptive adjustment enables the algorithm to transition from broad-range exploration to fine-grained local search, facilitating convergence toward the global optimum.

3.2.2 Network Reconfiguration Model Solving Process

The process of solving the new distribution network reconfiguration model based on the caterpillar fungus optimizer is as follows:

- Generate the initial population of caterpillar fungus using the distribution network topology and switch set as control variables.
- Calculate the initial power flow of the network. Compute the initial fitness of the caterpillar fungus population based on the objective function, and sort the individuals in descending order of fitness.
- The caterpillar fungus population explores hosts according to the wave advance operator and spiral rising operator, updates their positions, and records the best individual and the best result in the current generation. The best individual represents the optimal network reconfiguration strategy, and the best result includes the lost load, number of switching operations, and network losses.
- The caterpillar fungus performs parasitism behavior, update their parasitic positions until the maximum number of iterations is reached, and output the optimal network reconfiguration strategy.

For an explicit illustration, the pseudo-code of CFO for network reconfiguration model solving is provided in Table 2.

Table 2: Pseudo-code of CFO.

Algorithm 2: Network reconfiguration model solving algorithm based on CFO

Generate the initial population of caterpillar fungus;
Calculate the fitness value based on X_{CF} according to objective function;
FOR $iteration$ = 1: $Max\_iteration$
    FOR i = 1: N
        sort the individuals in descending order of fitness;
        IF $rand$ < 0.5 THEN // Wave advance operator
            Calculate the new position $X_{\mathrm{CF},i}^{\mathrm{so}}$ of the ith caterpillar fungus by Eq. (30);
    ELSE // Spiral rising operator
      Calculate the new position $X_{\mathrm{CF},i}^{\mathrm{so}}$ of the ith caterpillar fungus by Eq. (32);
      Check and correct $X_{\mathrm{CF},i}^{\mathrm{so}}$ to be within the coefficient range;
      IF $f\left(X_{CF,i}^{\mathrm{SO}}\left(t+1\right)\right) < f\left(X_{best}\right)$
        Compute the fitness of each caterpillar fungus $f\left(X_{CF,i}^{\mathrm{SO}}\left(t+1\right)\right)$
        $X_{best} = X_{CF,i}^{\mathrm{SO}}\left(t+1\right)$
      END IF
      END IF
    END FOR
    FOR i = 1: N
        IF $rand$ < 0.5 THEN // Re-parasitism mechanism
          Calculate the new position $X_{\mathrm{CF},i}^{\mathrm{pl}}$ of the ith caterpillar fungus by Eq. (34)
        ELSE // Optimal parasitism
            Calculate the new position $X_{\mathrm{CF},i}^{\mathrm{pl}}$ of the ith caterpillar fungus by Eq. (35)
            Check and correct $X_{\mathrm{CF},i}^{\mathrm{pl}}$ to be within the coefficient range;
            IF $f\left(X_{\mathrm{CF},i}^{\mathrm{pl}}\left(t+1\right)\right) < f\left(X_{best}\right)$
              Compute the fitness of each caterpillar fungus $f\left(X_{\mathrm{CF},i}^{\mathrm{pl}}\left(t+1\right)\right)$
              $X_{best} = X_{\mathrm{CF},i}^{\mathrm{pl}}\left(t+1\right)$
            END IF
          END IF
        END FOR
      END FOR

The flowchart of the proposed load transfer method is shown in Fig. 4.

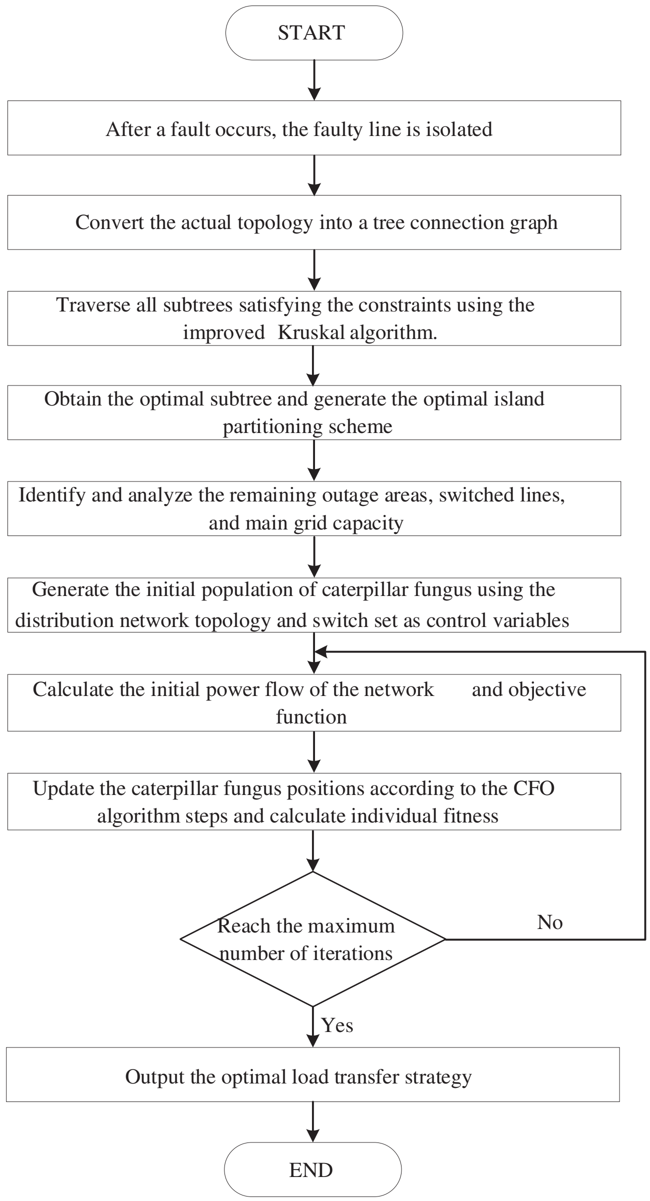

Figure 4: Flowchart of the proposed load transfer method.

4 Case Study

4.1 Case Conditions

The modified IEEE 33-bus system is utilized in this study as the novel distribution network system to verify the proposed optimal load transfer method. The system structure is shown in Fig. 5, with a rated voltage of 12.66 kV. The total active load and reactive power of the 33 buses are 3715 kW and 2300 kVar, respectively. The load classes and corresponding weights of each bus are listed in Table 3. The system consists of 37 power branches equipped with sectionalizing switches. The dashed lines represent tie lines, whose initial state is open, while all other switches are closed. The new distribution network integrates various distributed energy sources and adjustable power resources, where the initial state of charge of the distributed energy resource is set at full capacity. Three distributed PV systems are connected at buses 7, 11, and 17. The MT, the ESB, and the DE are connected at buses 13, 24, and 31, respectively. The integration details of adjustable power resources in the new distribution network are provided in Table 4.

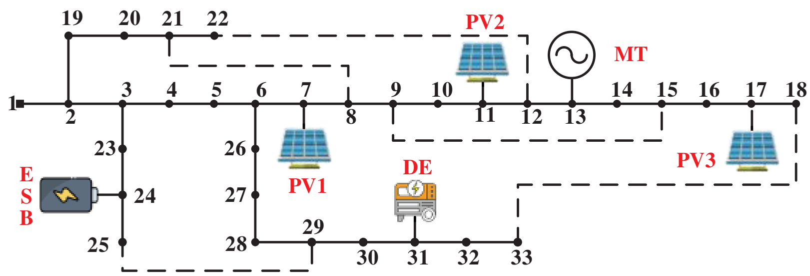

Figure 5: Structure of new distribution network test system.

Table 3: Load priority and weight of bus in the new distribution network.

Load Priority	Bus No.	Weight Coefficient
First-class load	5, 6, 12, 13, 23, 24, 29, 31	100
Second-class load	7, 11, 15, 22, 26, 30, 32	10
Third-class load	Others	1

Table 4: Integration of flexible resources in the novel distribution network.

Type	Equipment	DG No.	Bus No.	Capacity/kW	Characteristic Parameters
Source	MT	DG1	13	600	ramp rates: 300 kW/min
Source	DE	DG2	31	800	ramp rates: 400 kW/min
Source	PV1	DG3	7	200	power prediction
Source	PV2	DG4	11	100	power prediction
Source	PV3	DG5	17	150	power prediction
Load	Flexible load	/	5, 12, 16, 27	10% of rated power	/
Storage	ESB	DG6	24	1000	charging and discharging efficiencies: 90%

To cover two typical scenarios of distributed PV power generation (power peak and valley), fault occurrence is configurated at 12:00 and 21:00. For each fault scenario, two cases are considered including single-line fault (at branch 27–28) and simultaneous multi-line faults (at branches 8–9 and 20–21). After a fault occurs, the protection device first disconnects the faulty branch(es) to isolate the fault, resulting in power loss at downstream buses. During load transfer, island partitioning is performed according to the method explained in Section 2.3 to prioritize the restoration of critical loads. After separating the fault and islanded areas, the remaining network is reconfigured based on the model in Section 3.1 and solved using the CFO algorithm described in Section 3.2 to obtain the optimized network topology. The population size and maximum number of iterations for the CFO algorithm are set to 30 and 100, respectively.

4.2 Results and Analysis

4.2.1 Effectiveness Analysis of Load Transfer Strategy

Under the two fault scenarios, the Island partitioning results are shown in Table 5. When a fault occurs on branch 27–28 at 12:00, using the MT, DE, and ESB as black-start sources, three islands are formed. Island 1 contains 8 load buses (buses 11 to 18), island 2 contains 6 load buses (buses 28 to 33), and island 3 contains 3 load buses (buses 23 to 25), with total loads of 655, 800, and 930 kW, respectively. Since PVs are at its output peak at this time, it works together with the black-start sources to supply the islands. Therefore, the restored load in island 1 (which includes PV2 and PV3) exceeds the capacity of the MT alone, fully utilizing the available power. The total loads in the other two islands are close to, but do not exceed, the capacity of their respective black-start sources.

Table 5: Integration of flexible resources in the novel distribution network.

Time	Island Power Source	Load Buses in Island	Total Load	Switches Opened
12:00	DG1	11, 12, 13, 14, 15, 16, 17, 18	655 kW	Branch 10–11
	DG2	28, 29, 30, 31, 32, 33	800 kW	Branch 27–28
	DG6	23, 24, 25	930 kW	Branch 3–23
21:00	DG1	9, 10, 11, 12, 13, 14, 15, 16	525 kW	Branches 8–9, 16–17
	DG2	30, 31, 32, 33, 17, 18	770 kW	Branch 29–30
	DG6	23, 24, 25	930 kW	Branch 3–23

When simultaneous faults occur on branches 8–9 and 20–21 at 21:00, three islands are also formed. Island 1 contains 8 load buses (buses 9 to 16), island 2 contains 6 load buses (buses 30 to 33 and buses 17 to 18), and island 3 contains 3 load buses (buses 23 to 25), with total loads of 525, 770, and 930 kW, respectively. Since PVs output is negligible at this time, only the black-start sources provide power. To restore more load while ensuring operational security, the total load of each island is slightly less than the source capacity.

After island partitioning, the remaining network is reconfigured. The network reconfiguration status before and after reconfiguration is shown in Table 6. For the fault at 12:00, the network losses before and after reconfiguration are 83.4608 and 59.6767 kW, respectively, reduced by 23.7841 kW. For the fault at 21:00, the network losses before and after reconfiguration are 44.4177 and 21.2718 kW, respectively, reduced by 23.1459 kW, improving the economy of the network. After island partitioning, the remaining network has only 16 buses under both fault scenarios. The voltage distribution of the remaining network before and after reconfiguration is shown in Fig. 6. It can be seen that after network reconfiguration, the voltage magnitudes of buses with low voltage are raised. The minimum voltage magnitude increases from 0.9346 to 0.9610 p.u. for Fault 1, and from 0.9607 to 0.9824 p.u. for Fault 2, improving the power supply quality.

The final network topology after executing the load transfer strategy is shown in Fig. 7. The load transfer strategy varies depending on the fault time and fault branches. For Fault 1, a total of 3 switching operations are performed: opening branches 10–11, 3–23, and 27–28. For Fault 2, a total of 6 switching operations are performed: opening branches 8–9, 16–17, 3–23, and 29–30, and closing tie switches between buses 8–21 and 18–33.

Table 6: Results of the remaining network before and after reconfiguration.

Time	12:00		21:00	
Network Status	Before	After	Before	After
Network Losses (kW)	83.4608	59.6767	44.4177	21.2718
Total Number of Switch Operations	/	3	/	6
Minimum Voltage Magnitude (p.u.)	0.9346	0.9610	0.9607	0.9824

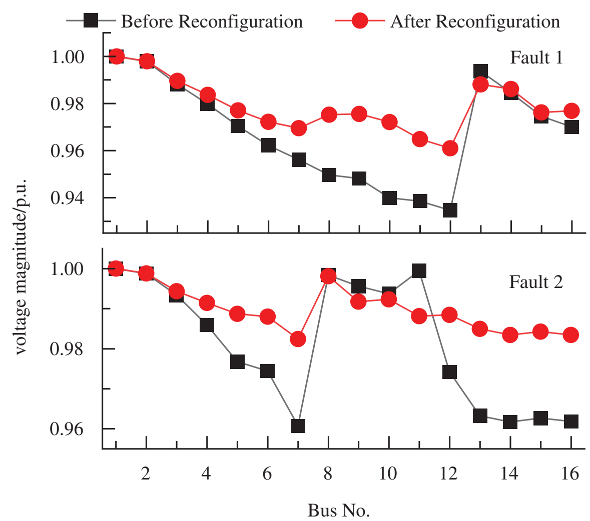

Figure 6: Voltage distribution before and after remaining network reconfiguration.

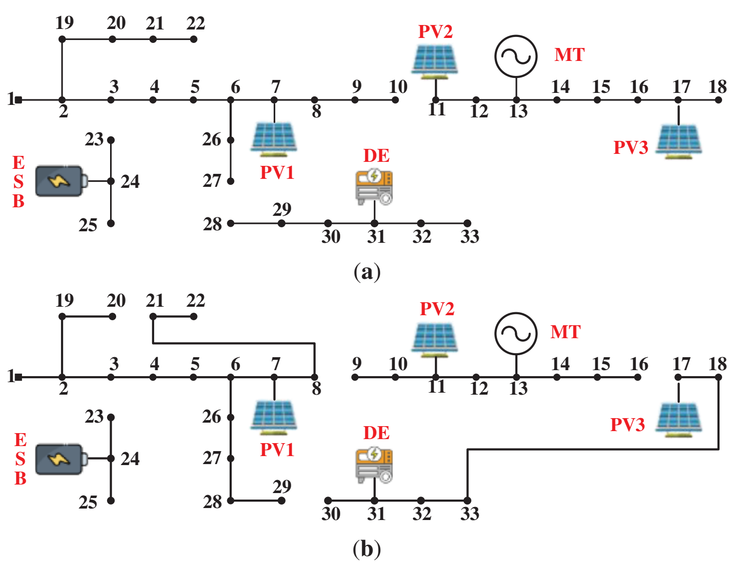

Figure 7: Topology of the new distribution network after load transfer. (**a**) Fault 1; (**b**) Fault 2.

To further demonstrate the superiority of the proposed load transfer strategy, two scenarios are set up for comparison. Strategy 1: A load transfer strategy that does not consider the Island operation capability of black-start sources in the new distribution network, performing network reconfiguration directly after a fault. Strategy 2: A load transfer strategy that implement only island partitioning without subsequent network reconfiguration. These are compared with the proposed Strategy 3 (integrated island partitioning and network reconfiguration). The load restoration is shown in Table 7. It can be seen that strategy 1, which performs network reconfiguration directly, treats the distribution network as a whole for power supply, resulting in higher total network losses. It can restore most loads but still leaves some loads de-energized. Strategy 2, which only performs Island partitioning, has smaller island networks and lower network losses, but a large number of loads remain outage. The proposed load transfer strategy (Strategy 3) combines island partitioning and network reconfiguration, achieving restoration of all loads in the network with relatively low losses. This hybrid approach ensures reliable power supply while validating its effectiveness and operational superiority contrast with standalone strategies. Moreover, in the proposed method, the total system losses for Fault 1 and Fault 2 are 100.23 and 67.56 kW, respectively, while the losses after reconfiguring the remaining network are 59.6767 and 21.2718 kW, respectively. It can be observed that the total system losses exceed the losses of the remaining network, which is due to the power losses also incurred in the islanded systems.

Table 7: Comparison of different load transfer strategies.

Time	**12:00**			**21:00**		
Strategy	**1**	**2**	**3**	**1**	**2**	**3**
Total Network Losses (kW)	142.43	40.56	100.23	137.47	46.29	67.56
Total Number of Switch Operations	2	3	3	2	4	6
Load Restoration Rate (%)	83.63	61.51	100	76.28	60.70	100

4.2.2 Performance Analysis of CFO-Based Solution for Network Reconfiguration

To validate the superiority of CFO in solving the network reconfiguration model, it is compared with commonly used heuristic algorithms: genetic algorithm (GA), particle swarm optimization (PSO), and whale optimization algorithm (WOA). Taking the solution of the remaining network reconfiguration model under fault 1 as an example, all algorithms are iterated 100 times. Fig. 8 shows the fitness curves of the four heuristic algorithms versus the number of iterations. It can be seen that, thanks to the unique optimization mechanism of the CFO, it can quickly approach the optimal solution, does not fall into local optima, has small solving error, and good optimization effect. The other three algorithms are prone to falling into local optima when faced with complex nonlinear optimization models, and their solving errors are also larger. In terms of solving time, the solving times for CFO, GA, PSO, and WOA are 8.62 s, 21.35 s, 17.59 s, and 19.48 s, respectively. The CFO reduces the solving time and greatly improves solving efficiency. Therefore, the CFO demonstrates good performance in both optimality and solving efficiency for the network reconfiguration model proposed in this paper.

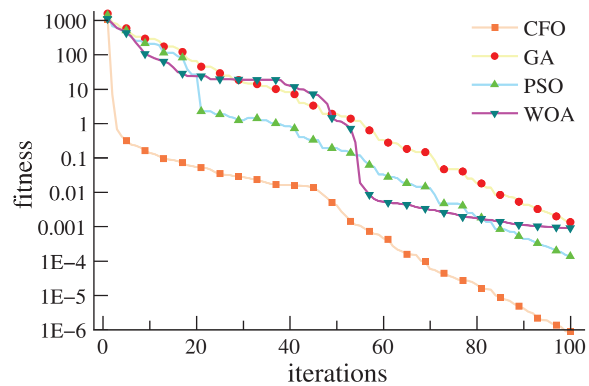

Figure 8: Performance comparison of four heuristic algorithms.

4.2.3 Adaptability Test for Large-Scale New-Type Distribution Networks

To demonstrate the applicability of the proposed load transfer technology to large-scale new distribution networks, further tests were conducted using the modified IEEE 123-bus system. The system was configured with five tie lines and integrated with 20 PVs, 4 MTs, 4 MTs, and 4 ESBs. 20 flexible load buses were also set. One hundred single-line fault scenarios were randomly generated, and real-time PVs output values were randomly sampled within 10% to 100% of the rated PVs capacity. Real-time load transfer was performed using the three aforementioned strategies, and the average values of relevant metrics over the 100 cases are presented in Table 8. The optimal solutions and total computation times obtained by the four heuristic algorithms for solving the 100 network reconfiguration models are shown in Fig. 9.

Table 8: Comparison of different load transfer strategies in large-scale new distribution networks.

Strategy	1	2	3
Average Total Network Losses (kW)	761.85	324.37	461.45
Average Total Number of Switch Operations	4.31	4.71	5.42
Average Load Restoration Rate (%)	68.15	45.58	96.28
Total Strategy Formulation Time (s)	16,874	453	3929

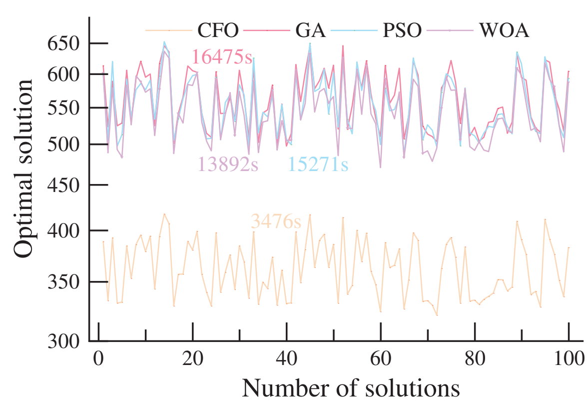

Figure 9: Real-Time optimization solutions of four heuristic algorithms in large-scale new distribution networks.

It can be observed that in large-scale new distribution systems, relying solely on either network reconfiguration or island partitioning would result in a significant amount of outage load. Although the proposed method increases the number of switching operations, it achieves an average load recovery rate of 96.28%, ensuring high-quality and highly reliable power supply with relatively low network losses. Furthermore, directly performing network reconfiguration, due to the complexity and scale of the model, required an average solving time of 168.74 s per case. In contrast, the proposed method, which performs reconfiguration on the remaining network after rapid island partitioning, reduces model complexity and significantly accelerates the solving efficiency, requiring only 39.29 s on average to provide a transfer strategy. Additionally, when dealing with the large-scale nonlinear model, the CFO algorithm spent an average of 34.76 s to solve one reconfiguration model and achieved a smaller objective function value compared to the other algorithms. This indicates that CFO can effectively escape local optima and converge to the optimal solution with a relatively fast iteration speed. The other common heuristic algorithms were prone to getting trapped in local optima and had slower iteration speeds, requiring average solving times of 164.75, 152.71, and 138.92 s per model while yielding larger objective function values. Compared to CFO, these solutions were non-optimal and exhibited poorer performance, making them unsuitable for large-scale nonlinear models.

5 Conclusion

Considering that the DGs in new distribution networks possess the capability of black-start, this paper proposes an optimal load transfer method for the new distribution network. The method incorporates the islanded operation of DGs and the reconfiguration of the remaining network. Experiential studies were conducted based on a modified IEEE 33-bus system, leading to the following conclusions:

(1) The improved Kruskal algorithm is developed to achieve optimal island partitioning for black-start power sources of distributed generators. The algorithm can better prioritize the restoration of power supply for critical loads.
(2) Compared to conventional heuristic algorithms, the proposed CFO algorithm demonstrates superior performance in escaping local optima and rapidly solving complex nonlinear models of network reconfiguration.
(3) In contrast to standalone methods that consider merely islanded operation or network reconfiguration, the proposed combined load transfer method can better ensure reliable power supply for various flexible loads. The proposed method can also achieve improved economic operation results during load transfer in new distribution networks.

Future research will further consider the complex characteristics of new distribution networks, including three-phase unbalance, meshed operation, and practical protection constraints.

Acknowledgement: We would like to express our gratitude to all members of the research group for their hard work.

Funding Statement: This work was supported by the Incubation Project of the State Grid Jiangsu Electric Power Co., Ltd. (JF2025017, Research and Development of an Emergency Load Transfer System for Multi-Scenario and Multi-Type Loads in Distribution Networks).

Author Contributions: The authors confirm contribution to the paper as follows: research concept and design: Zhan Lv, Lan Lan, Zijian Hu; data collection: Honghua Xu, Hong Zhu; analysis and interpretation of results: Zhan Lv, Zijian Hu, Jiehua Hou; manuscript preparation draft: Zhan Lv, Lan Lan. All authors reviewed and approved the final version of the manuscript.

Availability of Data and Materials: The authors confirm that the data supporting the findings of this study are available within the article.

Ethics Approval: Not applicable.

Conflicts of Interest: The authors declare no conflicts of interest.

References

1. Yang H, Deshmukh R, Suh S. Global transcontinental power pools for low-carbon electricity. Nat Commun. 2023;14(1):8350. doi:10.1038/s41467-023-43723-z.
2. Gao Y, Ai Q, Yousif M, Wang X. Source-load-storage consistency collaborative optimization control of flexible DC distribution network considering multi-energy complementarity. Int J Electr Power Energy Syst. 2019;107(1):273–81. doi:10.1016/j.ijepes.2018.11.033.
3. Rathore A, Patidar NP. Optimal sizing and allocation of renewable based distribution generation with gravity energy storage considering stochastic nature using particle swarm optimization in radial distribution network. J Energy Storage. 2021;35(1):102282. doi:10.1016/j.est.2021.102282.
4. Ghasemi S, Mohammadi M, Moshtagh J. A new look-ahead restoration of critical loads in the distribution networks during blackout with considering load curve of critical loads. Electr Power Syst Res. 2021;191(2):106873. doi:10.1016/j.epsr.2020.106873.
5. Wang R, Ji H, Li P, Yu H, Zhao J, Zhao L, et al. Multi-resource dynamic coordinated planning of flexible distribution network. Nat Commun. 2024;15(1):4576. doi:10.1038/s41467-024-48862-5.
6. Li Y, Wang D. Whole-line fault analysis method for unbalanced distribution networks with inverter interfaced distributed generators. IET Gener Transm Distrib. 2022;16(15):3016–26. doi:10.1049/gtd2.12493.
7. Li H, Yan J, Liu Y. A link-path model-based load-transfer optimization strategy for urban high-voltage distribution power system. IEEE Access. 2020;8:3728–37. doi:10.1109/ACCESS.2019.2960297.
8. Li Z, Zhang Y, Aqeel Ashraf M. Optimization design of reconfiguration algorithm for high voltage power distribution network based on ant colony algorithm. Open Phys. 2018;16(1):1094–106. doi:10.1515/phys-2018-0130.
9. Oh JY, Oh S, Lee GS, Yoon YT, Jo S. Sequential control of individual switches for real-time distribution network reconfiguration using deep reinforcement learning. IEEE Trans Smart Grid. 2025;16(5):3666–83. doi:10.1109/TSG.2025.3580063.
10. Monteiro RVA, Bonaldo JP, Da Silva RF, Bretas AS. Electric distribution network reconfiguration optimized for PV distributed generation and energy storage. Electr Power Syst Res. 2020;184(3):106319. doi:10.1016/j.epsr.2020.106319.
11. Bai L, Jiang T, Li F, Chen H, Li X. Distributed energy storage planning in soft open point based active distribution networks incorporating network reconfiguration and DG reactive power capability. Appl Energy. 2018;210(2):1082–91. doi:10.1016/j.apenergy.2017.07.004.
12. Hanashiro R, Tsuji T, Moriuchi E, Fujita N, Ishibashi K. Network reconfiguration method considering probabilistic operation of SVR in a distribution system. IEEJ Trans Electr Electron Eng. 2025;10(2):70223. doi:10.1002/tee.70223.
13. Basso TS, DeBlasio R. IEEE 1547 series of standards: interconnection issues. IEEE Trans Power Electron. 2004;19(5):1159–62. doi:10.1109/TPEL.2004.834000.
14. Zhao Y, Zhang T, Sun L, Zhao X, Tong L, Wang L, et al. Energy storage for black start services: a review. Int J Miner Metall Mater. 2022;29(4):691–704. doi:10.1007/s12613-022-2445-0.
15. Ma L, Hui H, Wang S, Song Y. Coordinated optimization of power-communication coupling networks for dispatching large-scale flexible loads to provide operating reserve. Appl Energy. 2024;359(1):122705. doi:10.1016/j.apenergy.2024.122705.
16. Li Y, Xiao J, Chen C, Tan Y, Cao Y. Service restoration model with mixed-integer second-order cone programming for distribution network with distributed generations. IEEE Trans Smart Grid. 2019;10(4):4138–50. doi:10.1109/TSG.2018.2850358.
17. Wan D, Zhao M, Yi Z, Jiang F, Guo Q, Zhou Q. Mixed-integer second-order cone programming method for active distribution network. Front Energy Res. 2023;11:1259445. doi:10.3389/fenrg.2023.1259445.

18. Chen C, Wu Y, Cao Y, Liu S, Tan Q, Wang W. Intending island service restoration method with topology-powered directional traversal considering the uncertainty of distributed generations. Front Energy Res. 2021;9:762491. doi:10.3389/fenrg.2021.762491.
19. Rodríguez-Montañés M, Rosendo-Macías JA, Gómez-Expósito A. A systematic approach to service restoration in distribution networks. Electr Power Syst Res. 2020;189(6):106539. doi:10.1016/j.epsr.2020.106539.
20. Huang Y, Li G, Chen C, Bian Y, Qian T, Bie Z. Resilient distribution networks by microgrid formation using deep reinforcement learning. IEEE Trans Smart Grid. 2022;13(6):4918–30. doi:10.1109/TSG.2022.3179593.
21. Si R, Chen S, Zhang J, Xu J, Zhang L. A multi-agent reinforcement learning method for distribution system restoration considering dynamic network reconfiguration. Appl Energy. 2024;372(7):123625. doi:10.1016/j.apenergy.2024.123625.
22. Yang X, Li L, Fu J, Han Y, Li Z. Two-stage power restoration in interconnected and islanded distribution networks. J Shanghai Univ Electr Power. 2024;40:58–65. (In Chinese).
23. AlOwaifeer M, AlMuhaini M. Load priority modeling for smart service restoration. Can J Electr Comput Eng. 2017;40(3):217–28. doi:10.1109/cjece.2017.2705174.
24. Cheng LL, Luo ZJ, Li Q, Zhang NY, Li YR, Zang HX. Real-time stochastic dispatch method for active distribution network using fuzzy neural network pre-decision. Autom Electr Power Syst. 2025;49(19):75–85. (In Chinese). doi:10.7500/AEPS20250213005.
25. Feng XP, Song XH, Liang Y, Meng XL. Islanding method based on minimum spanning tree and improved genetic algorithm for distribution system with DGs. High Volt Eng. 2015;41(10):3470–8. (In Chinese). doi:10.13336/j.1003-6520.hve.2015.10.039.
26. Lu D, Li W, Zhang L, Fu Q, Jiao Q, Wang K. Multi-objective optimization and reconstruction of distribution networks with distributed power sources based on an improved BPSO algorithm. Energies. 2024;17(19):4877. doi:10.3390/en17194877.
27. Yang B, Liang B, Zhou S, Qian Y, Zheng R, Shu H, et al. A novel bio-inspired caterpillar fungus (*Ophiocordyceps sinensis*) optimizer for SOFC parameter identification via GRNN. Renew Energy. 2026;256(6):123995. doi:10.1016/j.renene.2025.123995.